A&A 459, 265–270 (2006)
DOI: 10.1051/0004-6361:20065586

Astronomy & Astrophysics

Seasonal variations of the martian CO over Hellas as observed by OMEGA/Mars Express

Th. Encrenaz[1], T. Fouchet[1], R. Melchiorri[1], P. Drossart[1], B. Gondet[2], Y. Langevin[2], J.-P. Bibring[2], F. Forget[3], and B. Bézard[1]

[1] LESIA, UMR-CNRS 8109, Observatoire de Paris, 92195 Meudon, France
e-mail: therese.encrenaz@obspm.fr
[2] Institut d'Astrophysique Spatiale, Orsay Campus, 91405 Orsay, France
[3] IPSL/LMD, place Jussieu, 75231 Paris Cedex 05, France

Received 11 May 2006 / Accepted 4 August 2006

ABSTRACT

The OMEGA imaging spectrometer aboard Mars Express has been used to study the evolution of the CO abundance over the Hellas basin, as a function of the seasonal cycle. In spite of significant uncertainties, due to the low intensity of the (2−0) CO band at 2.3 μm, these data allow to search for spatial variations over Hellas, where the surface pressure and the CO band depth are maximum. The OMEGA data suggest an enhancement over Hellas at $Ls = 130-150$ deg (end of southern winter), by a factor of about 2 with regard to $Ls = 330-350$ deg (end of northern summer). This behavior is to be compared with the evolution of argon, another non-condensible species which also shows strong variations with Ls at southern latitudes (Sprague et al. 2004). This result appears also consistent with the GCM predictions which indicate an enrichment by a factor of about 2 of non-condensible species over Hellas during southern winter (Forget et al. 2006).

Key words. planets and satellites: individual: Mars – infrared: solar system

1. Introduction

Ground-based observations of CO on Mars have been performed for almost 30 years, both in the infrared range (Kaplan et al. 1977) and in the millimeter range (Kakar et al. 1977). The CO (1−0) and (2−1) millimeter transitions have been observed using heterodyne spectroscopy, together with the ^{13}CO (1−0) and (2−1) transitions, to constrain the CO mixing ratio and the mean temperature profile (see, e.g. Clancy et al. 1990; Lellouch et al. 1991). A mean CO value of 800 +/− 200 ppm(v) was inferred, with no evidence for spatial nor temporal variations larger than 40 percent. Infrared spectroscopic observations of the (1−0) and (2−0) vibrational bands of CO, at 4.7 μm and 2.35 μm respectively, led to comparable results (Billebaud et al. 1992, 1998). A lower value, closer to 600−700 ppm, has been retrieved from a recent re-analysis of the millimeter data (Clancy et al. 2006).

A seasonal variation of the CO mixing ratio could be expected, since CO is a non-condensible species whereas CO_2 is subject to a seasonal condensation which modulates the global pressure by about 30 percent. Such an effect was first noticed by Krasnopolsky (2002) who reported latitudinal variations of the CO mixing ratio from 800 ppm north of 23N up to 1200 ppm at 50S latitude during early northern summer ($Ls = 112$ deg). The seasonal variation of argon, another non-condensible species, has been also detected by the Gamma Ray Spectrometer (GRS) aboard Mars Odyssey (Sprague et al. 2004). An enhancement by a factor as high as 6 was reported at high southern latitudes during southern winter (Sprague et al. 2004).

A detailed model of the enrichment of non-condensible gas during the condensation of polar caps (and their dilution during the cap sublimation) has been developed within the LMD Global Climate Model (Forget et al. 1999) which is able to simulate the transport of tracer gas like CO in the atmosphere (Forget et al. 2006). In its baseline version, this model also includes a parametrisation of the CO_2 condensation-sublimation which estimates the amount of CO_2 that condenses or sublimes on the surface or in the atmosphere, at every model time step. On this basis, the corresponding increase or decrease in mixing ratio for the non-condensible gas (N_2, Ar, CO, etc.) at every grid point was exactly computed taking into account the numerical effect of atmospheric condensation on the vertical coordinate $\sigma = p/p_s$ that is used in such a model (the algorithm is described in Forget et al. 2006). Since the mean molecular weight of the non-condensible gas is only 32.3 g mol^{-1}, compared to 44 g mol^{-1} for CO_2, the enrichment near the surface where most of the CO_2 condenses induces deep static instability and vertical mixing. These effects are taken into account assuming that vertical instability and convection occur if $\delta\theta m/\delta z$ is negative, with θ the potential temperature, m the local air mean molecular mass and z the altitude.

Simulations performed for several martian years show a clear enrichment during the polar night in both hemispheres, especially in the first hundreds of meters above the surface. The model is found to accurately predict the argon enrichment detected by Sprague et al. (2006) in the northern hemisphere. In the southern hemisphere however, the GCM simulations underestimate the argon enrichment south of 75S, probably because of a strong overestimation of the southern polar night temperature (a well-known issue in Mars GCM climatology), leading to unrealistic mixing between the southern polar region and lower latitudes in winter. This meteorological problem is not thought to strongly affect the prediction of the climate in the Hellas area,

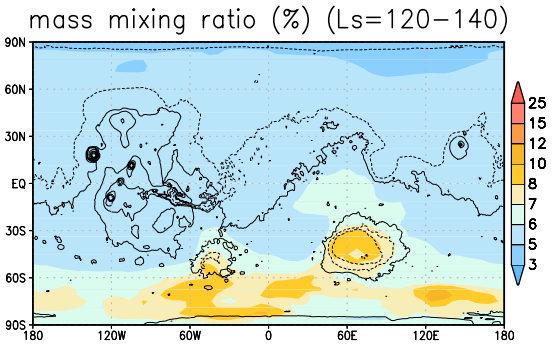

Fig. 1. A map of the column averaged mass mixing ratio (percent of kg/kg) of non-condensible species during southern winter ($Ls = 120-140$ deg), as simulated by the LMD Mars General Circulation Model. The figure is taken from Forget et al. (2006). A doubling of the non-volatile gas mixing ratio (like the CO mixing ratio) is predicted in the Hellas region.

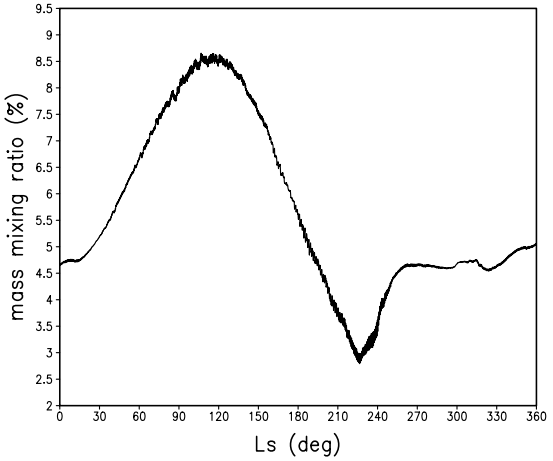

Fig. 2. Evolution of the mixing ratio of non-condensible species over the Hellas basin (35S, 65E) as a function of the solar longitude Ls. A doubling of the mixing rati is expected at $Ls = 90-150$ deg with respect to its value at $Ls = 270-10$ deg.

where the non-condensible gas mixing ratio reaches more than twice the mean atmospheric value (Fig. 1). This results from the fact that the atmosphere inside Hellas is well isolated by a local vortex and a stationary low pressure zone due to the stretching of vortex tubes of air passing over the Hellas topographic depression. The evolution with Ls of the mixing ratio of non-condensible species over Hellas is shown in Fig. 2.

In this paper, we present an analysis of the CO mixing ratio over Hellas as a function of Ls, using the OMEGA imaging spectrometer aboard the Mars Express orbiter. Observations and data analysis are described in Sect. 2. Our modelling procedure is shown in Sect. 3. Results are presented and discussed in Sect. 4. Our conclusions are summarized in Sect. 5.

2. Observations and data analysis

Aboard Mars Express, since January 2004, the OMEGA imaging spectrometer operates from 0.3 μm to 5.2 μm, with a spectral sampling of 14 nm in the 1.0–2.7 μm range. Its instantaneous field of view (IFOV) of 1.2 mrad corresponds to about 300 m at the martian surface near periapsis.

The 1.0–2.7 μm spectrum of Mars is dominated by signatures of CO_2, in particular two strong bands at 2.7 μm

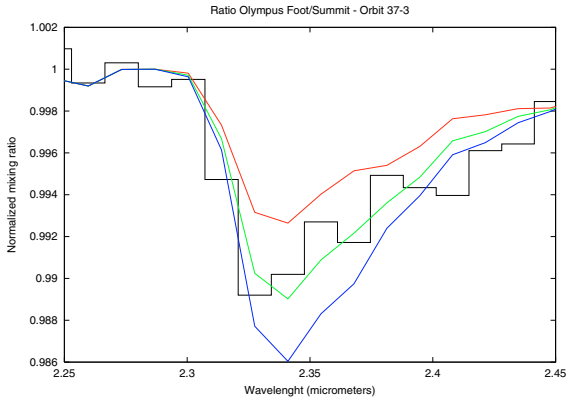

Fig. 3. Black curve: ratio of two averaged OMEGA spectra, recorded at the foot and at the summit of Olympus Mons respectively (Orbit 37-3), in the region of the CO 2.35 μm band. The summit spectrum, corresponding to the summation of 352 individual spectra, is taken as a reference. Color curves: synthetic ratios of spectra, using a radiative transfer code without scattering ($Ps = 1.1$ mbar at the summit, 6.5 mbar at the foot). From top to bottom; CO = 500, 1000 and 1500 ppm. The best fit corresponds to CO = 1000 +/− 400 ppm (+/− σ). Including a correction to account for scattering effects (see text), the result becomes CO = 1100 +/− 500 ppm.

and 2.0 μm. H_2O shows a clear signature at 2.6 μm, and CO exhibits its two vibrational bands (1−0) and (2−0) at 4.7 μm and 2.35 μm respectively. The (1−0) CO band is stronger, however it is formed in the thermal regime. As a result, it cannot be used when the surface temperature is too low, in particular, at high latitude during winter. For this reason, we have used the (2−0) CO band at 2.35 μm which appears in the reflected part of the spectrum.

In a previous analysis of the OMEGA spectra, we have used the 2.6 μm band of H_2O to monitor its column density (Encrenaz et al. 2005; Melchiorri et al. 2006). In this analysis, in order to eliminate the uncertainty associated with the OMEGA instrumental transfer function, we have divided each individual spectrum by the averaged spectrum of the Olympus summit, taken as a reference. We follow the same procedure in the present study.

Figure 3 shows the retrieved CO mixing ratio in the vicinity of Olympus Mons, using the above technique. A mean spectrum recorded along Orbit 37-7, for latitudes ranging from 25N to 32N, has been divided by our reference spectrum, taken at the summit of Olympus Mons. The surface pressure of the reference spectrum has been inferred from an interpolation of the MOLA data within the high-resolution grid of the Global Climate Model developed at Oxford University and the Laboratoire de Meteorologie Dynamique (Forget et al. 1999). A comparison with synthetic models (see below the description of the modelling procedure) shows that the CO mixing ratio, at this location and for $Ls = 337$ deg, is 1100 +/− 500 ppm. In spite of its weak depth (about 1 percent), the CO band is reasonably well fitted by the models, because the two sites are close enough to show no variation in terms of mineralogy. Taking into account the large error bars, our result, although not inconsistent with previous determinations of the CO mixing ratio on Mars, seems to indicate a higher value than previously reported. This result is discussed in more detail in Sect. 4.

In the case of the water analysis, we were able to set up an automatic method, which provides a direct retrieval of the water column density from the measurement of the depth of the H_2O band at 2.6 μm. However, the depth of the water band was ranging between about 3 to 10 percent, depending upon the

Table 1. Summary of OMEGA observations and inferred CO mixing ratios over Hellas.

Orbit	*Ls*	*P*s (mbar)	Airmass	CO (ppm, +/− σ)
30-1	335.7	10.0	1.17	970 +/– 370
41-3	337.9	10.0	1.20	810 +/– 360
47-1	339.0	10.0	1.20	760 +/– 360
284-0	16.6	11.5	1.15	1000 +/– 400
422-1	36.1	12.0	1.75	1220 +/– 370
521-1	48.5	13.5	2.25	1220 +/– 520
554-1	52.6	13.5	2.70	1550 +/– 500
1186-4	132.0	11.5	1.52	2770 +/– 770
1241-5	139.5	10.5	1.52	1890 +/– 590
1935-4	251.7	10.0	1.55	1640 +/– 640
1946-4	253.6	10.0	1.47	1290 +/– 690
2177-4	295.9	9.7	1.55	1020 +/– 570

season and location. As illustrated above, the CO band at 2.35 μm has typical depths ten times smaller. The large uncertainty of our measurement for Orbit 37-3 illustrates that it is not possible to obtain a global map of CO using the same method as for H_2O. Thus, we have limited our analysis to the Hellas basin for two reasons: (1) as it corresponds to lowest altitudes, the CO band depth is maximum; (2) as mentioned above, maximum seasonal variations are expected in this region according to GCM predictions. Table 1 lists the selected observations with their observing parameters and the retrieved CO mixing ratios. The retrieval procedure is discussed below (Sect. 3).

In what follows, we have used two references (both corresponding to Olympus summit), depending on the integrating time of the data. Spectra recorded with 2.5 ms integrating times (orbits 1935 and above) have been divided by the reference of Orbit 37-3, also recorded at 2.5 ms. For data recorded at 5 ms (orbits 30 to 1241), we have used a reference taken at Orbit 501-4, also registered with 5 ms integration time.

3. Modelling of the atmospheric spectrum

3.1. Radiative transfer without scattering

In a first step, the absorption due to the martian atmospheric gases was calculated over the 1.0−2.7 μm range, using a line-by-line radiative transfer code, without scattering by aerosols, which includes the spectral signatures of CO_2, H_2O and CO (Encrenaz et al. 2005). The surface pressure and the temperature profile over Hellas were taken from the Global Climate Model (GCM) developed at LMD-Oxford (Forget et al. 1999). While the choice of the surface pressure is critical for the determination of the CO mixing ratio, the choice of the thermal profile is much less critical as the line is formed in reflected sunlight. For each observation listed in Table 1, we have calculated a set of synthetic spectra corresponding to its surface pressure, its temperature profile and its airmass, for CO varying from 500 to 3000 ppm. The inferred CO mixing ratio and its error bars (+/− σ) has been obtained from a least-square procedure. We have checked that our modelling of the CO_2 using the MOLA surface pressure provides a good fit of the observed spectrum (Fig. 4). However, in some cases, the core of the strong CO_2 band at 2.0 μm shows some discrepancy between the synthetic and observed curves, with the modelled spectrum being deeper. This effect is visible when dust is present in the atmosphere, as our model does not include scattering.

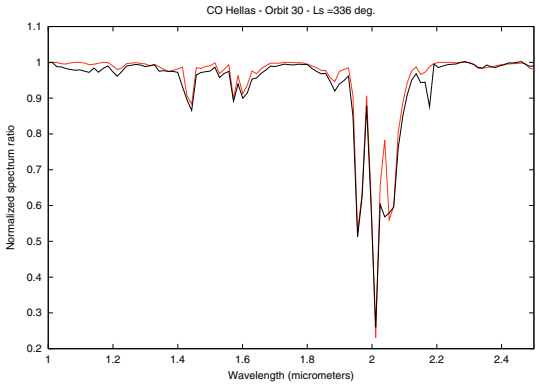

Fig. 4. An example of averaged spectrum over the Hellas region, divided by the reference spectrum taken at the summit of Olympus Mons. The Hellas spectrum corresponds to Orbit 30-1 (*Ls* = 336 deg). The discrepancy at 2.05 μm is due to a bad pixel in the OMEGA data. Color curves: synthetic ratio.

3.2. Correction due to aerosol scattering

In order to quantify the effect of dust scattering, we have used a radiative transfer code including scattering by aerosols to model both the CO (2−0) band at 2.3 μm and the CO_2 band at 2.0 μm. Synthetic models including dust multiple scattering were created using a two-stream radiative transfer code. Specifically, the atmosphere was divided in 45 layers equally spaced in ln *P*. The reflexion and transmission coefficients were calculated for each layer, then the upward and downward fluxes were calculated assuming the usual continuity conditions at the boundary of two layers. The upward and downward fluxes were used to calculate the source function in each layer. The radiative transfer equation was finally integrated along the outgoing ray path. The dust scattering properties were assumed similar to that derived by Ockert-Bell et al. (1997), i.e. $\omega_0 = 0.95$ and $g = 0.67$ (with ω_0 the single scattering albedo and g the asymmetry factor of the phase function). The dust was assumed to be well mixed with the atmospheric gas. This multiple scattering code was coupled to a correlated-k model to account for the gas absorptions. The correlated-k coefficients were calculated from the line by line opacities presented above.

Because such calculations are time-consuming, we have performed a sensitivity study by choosing a surface pressure of 10 mbars, 6 values of the CO mixing ratio (from 500 to 3000 ppm), and 4 values of the depth optical depth (0.0, 0.2, 0.5 and 1.0). Results are shown in Figs. 4 and 5. It can be seen that, for all values of the CO mixing ratio, the effect of the aerosol scattering lowers the depth of the CO band by about 3 percent, 8 percent and 18 percent for optical depths of 0.2, 0.5 and 1.0 respectively (Fig. 5). The same effect is observed for the 2.0 μm band of CO_2 (Fig. 6). In order to estimate the dust opacity corresponding to each observation, we have used the GCM predictions for a nominal model of the dust, and we have checked that these values fit the core the CO_2 band in the OMEGA spectra. In order to derive the uncertainty associated to the dust opacities, we have conservatively used the values of the GCM "dusty model" as an upper limit, and zero as a lower limit. We have corrected the values inferred from our first-step analysis (Sect. 3.1) using the nominal values of the dust opacities, and we have enlarged our error bars accordingly. As a result, our CO mixing ratios are enlarged by factors ranging between 8 and 17 percent according to the various cases. Final results are summarized in Table 1.

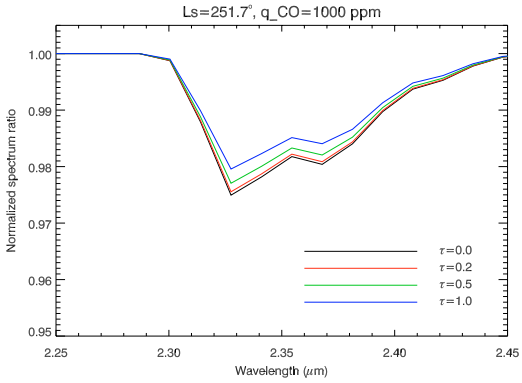

Fig. 5. Effect of dust scattering on the depth of the CO band at 2.35 μm. The surface pressure is 10 mbars, the CO mixing ratio is 1000 ppm. Dust opacity, *from top to bottom*: 1.0, 0.5, 0.2 and 0.0.

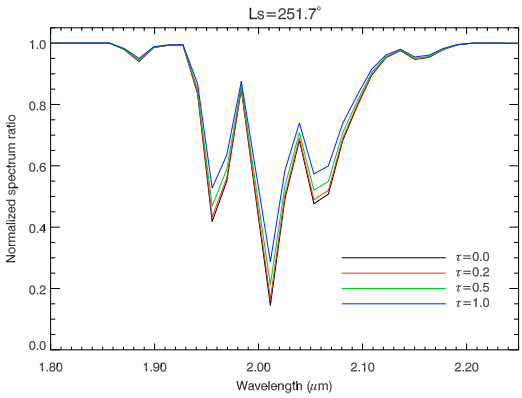

Fig. 6. Effect of dust scattering on the depth of the CO_2 band at 2.0 μm. The surface pressure is 10 mbars. Dust opacity, *from top to bottom*: 1.0, 0.5, 0.2, 0.0.

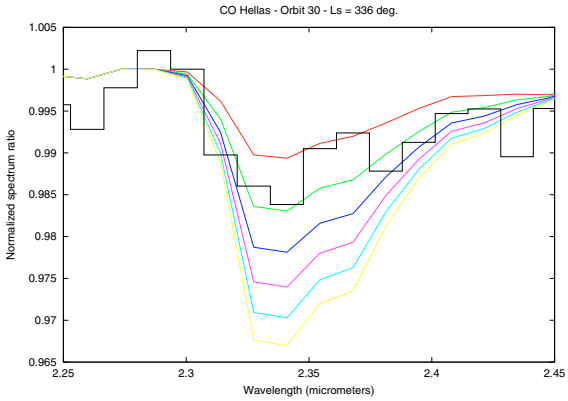

Fig. 7. Black curve: the averaged observed spectrum over Hellas for $Ls = 335.7$ deg (orbit 30-1) divided by the reference spectrum taken at the summit of Olympus Mons. Color curves: synthetic ratio of spectra, calculated for the surface pressure and the airmass of the observation, with, *from top to bottom*: CO = 500, 1000, 1500, 2000, 2500 and 3000 ppm.

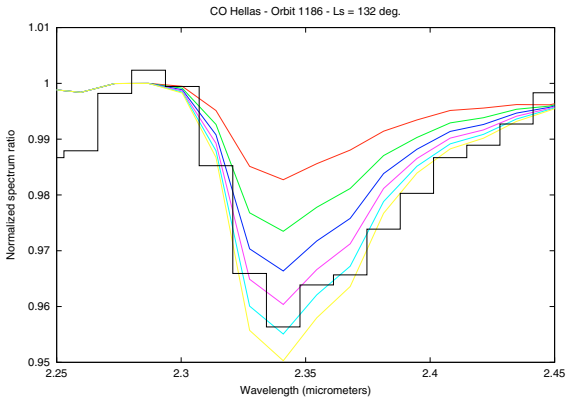

Fig. 8. Black curve: the averaged observed spectrum over Hellas for $Ls = 132.0$ deg (orbit 1186-4) divided by the reference spectrum. Models: see Fig. 7.

4. Results and discussion

4.1. Variations of the CO mixing ratio with Ls

Our results are illustrated in Figs. 7−10, which show the evolution of the depth of the CO (2−0) band as a function of *Ls*. Note that these figures show the OMEGA spectra compared with radiative transfer models without scattering; they are shown to illustrate the evolution of the CO band as a function of season. At the beginning of the mission, we are close to the equinox and the CO band is relatively weak. Then the CO band depth increases as we move toward southern winter with a maximum around $Ls = 132$ deg. It decreases again at $Ls = 254$ deg as we have passed again the equinox. The absence of data in some regions is due to observational constraints. Our results, including the correction by dust scattering, are also summarized in Table 1 and Fig. 11, which show the CO mixing ratio as a function of *Ls* over Hellas and over two other northern areas (see Sect. 4.3). Above Hellas, it can be seen that, between $Ls = 130$ and 180 deg (end of southern winter), a CO enhancement by a factor about 2 is observed with respect to the minimum value of about 1000 ppm, observed at 330−350 deg (end of southern summer).

It can be seen from Fig. 11 that the mean value of the CO mixing ratio over Hellas is larger than the previous values typically retrieved from ground-based measurements. This may be due to the fact that all values are scaled with respect to the CO mixing ratio over Olympus Mons, which itself is high, and defined with a large error bar. However, this uncertainty should not affect our result concerning the seasonal variations of CO over Hellas.

4.2. Variations of the CO mixing ratio over the Hellas basin

We have seen that the CO mixing ratio over Hellas increases during southern winter, but we need to investigate whether or not this enhancement is localized over the Hellas basin. For this purpose, we have used Orbit 1186-4 which shows the maximum increase of CO, and we have studied the averaged spectrum at latitude 23S (Fig. 12). In spite of the large error bars, it can be seen that, at this location, the inferred mixing ratio (1100 +/− 500 ppm) is lower than its value at the bottom of the Hellas basin. This indicates that the enrichment appears to be confined to the Hellas basin itself, as predicted by the GCM calculations (Fig. 1; Forget et al. 2006).

4.3. An estimate of the CO mixing ratio at northern latitudes

We have also tried to determine if the CO mixing ratio could be measured in the northern hemisphere. For this purpose, in order to maximize the CO band depth, we have selected two areas, N1 (60N, 350E) and N2 (45N, 110E), where the altitude is minimum. Only a few orbits were available over these two

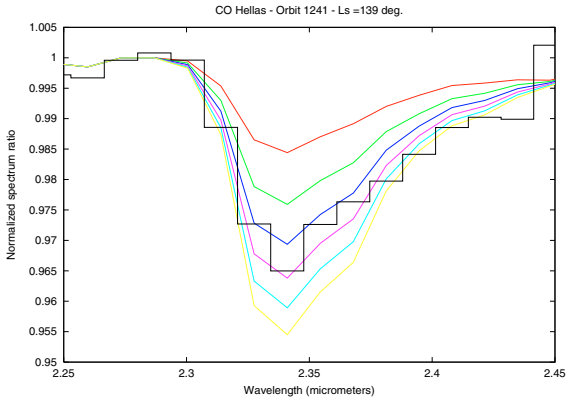

Fig. 9. Black curve: the averaged observed spectrum over Hellas for $Ls = 139.5$ deg (orbit 1241-5) divided by the reference spectrum. Models: see Fig. 7.

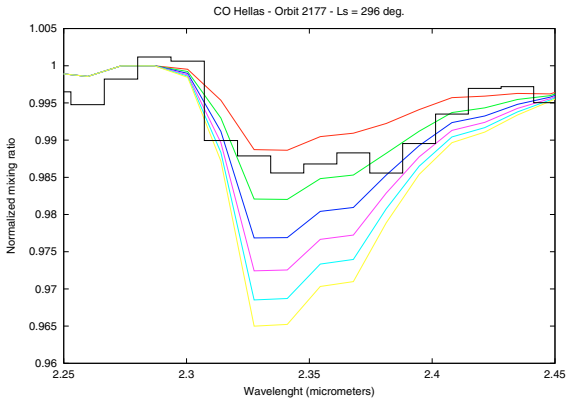

Fig. 10. Black curve: the averaged observed spectrum over Hellas for $Ls = 295.9$ deg (orbit 2177-4) divided by the reference spectrum. Models: see Fig. 7.

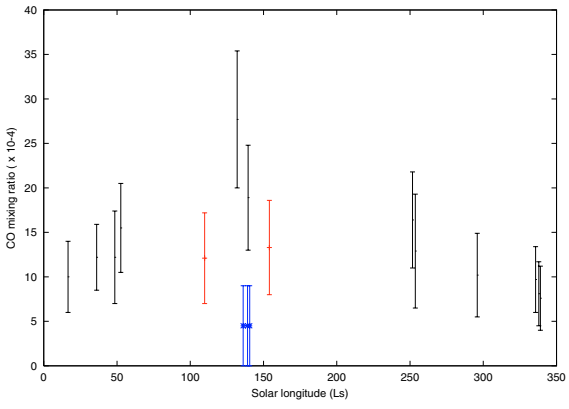

Fig. 11. Black curve: the CO mixing ratio as a function of the solar longitude, over different locations. Black: Hellas; red = N1 (60N, 350E); blue: N2 (45N, 110E).

regions; the observing parameters and the results are shown in Table 2.

In the case of Region N1, the two spectra give comparable CO mixing ratios, also close to the mean value observed over Hellas; an example is shown in Fig. 13. In contrast, a surprising result is obtained on Region N2, observed during 3 almost consecutive orbits. In all cases, the CO band is not detectable at all (Fig. 14). Taking into account the correction due to dust scattering, we find that the CO mixing ratio is lower than 900 ppm,

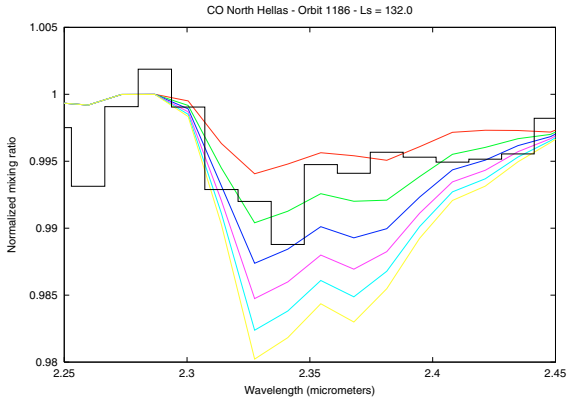

Fig. 12. Black curve: the averaged observed spectrum at the north of Hellas (lat. 23S) for $Ls = 132.0$ deg (orbit 1186-4) divided by the reference spectrum. Models: see Fig. 7.

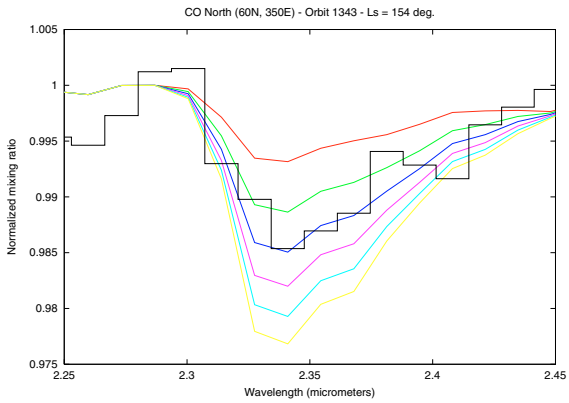

Fig. 13. The averaged observed spectrum over region N1 (60N, 350E), divided by the reference, for $Ls = 154.0$ deg (Orbit 1343-2). Models: see Fig. 7.

Table 2. OMEGA observations and inferred mixing ratios in the northern hemisphere.

Orbit	Ls	Ps (mbar)	Airmass	CO (ppm)
N1(60N,350E)				
1017-5	109.8	7.6	1.22	1210 +/– 510
1343-2	154.0	7.5	1.12	1330 +/– 530
N2(45N,110E)				
1216-0	136.1	7.5	1.12	450 +/– 450
1238-2	139.1	7.5	1.12	450 +/– 450
1249-2	140.6	7.5	1.40	450 +/– 450

i.e. significantly lower than the value inferred over Hellas for the same value of Ls. This result appears in agreement with the dynamical seasonal phenomenon described by Forget et al. (2006). In contrast, we cannot drive any conclusion about the behaviour of CO over the region N1. More data would be needed to retrieve information on possible seasonal and longitudinal effects in the northern hemisphere.

4.4. Comparison with models and ground-based observations

Our result is to be compared with the predicted evolution of the non-condensible species at high latitude, as calculated by the GCM model. Forget et al. (2006) have performed a parametrization of this phenomenon which predicts a significant

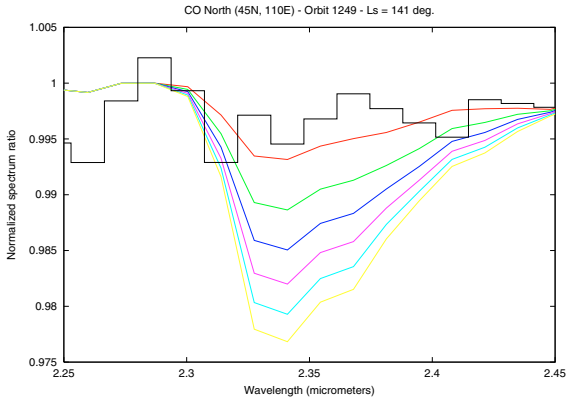

Fig. 14. The averaged observed spectrum over region N2 (45N, 110E), divided by the reference, for $Ls = 140.6$ deg (Orbit 1249-2). Models: see Fig. 7.

enhancement (by a factor about 2) of the non-condensible species at high latitude during winter ($Ls = 90-150$ deg; see Fig. 2). This enhancement seems more or less uniform with longitude at high northern latitudes. However, at high southern latitudes, the large topographic anomaly of the Hellas basin induces a strongly localized maximum over Hellas during southern winter (Fig. 1). Note that, in the GCM, a local minimum is expected for $Ls = 210-240$ deg (Fig. 2), a season for which no OMEGA data are available. To first order, our result seems to confirm the trend predicted by the GCM modelling. However, more data will be needed to confirm this effect.

We can also compare our results with the analysis performed by Krasnopolsky (2003) who used the C-SHELL imaging spectrograph at the NASA Infrared Telescope Facility (IRTF) to map the CO (3−0) band at 1.6 μm, for $Ls = 112$ deg. The author detected a north-south asymmetry, with a CO increase of 50 percent between 23N (CO = 830 ppm) to 50S (CO = 1240 ppm). This effect is interpreted as the consequence of CO_2 condensation during polar winter, leading to an accumulation of non-condensible species. We note that both studies disagree on the variation of CO over Hellas. Krasnopolky's study shows no significant variation inside and outside the basin, while our data show an increase by a factor about 2 between the bottom of Hellas and the northern edge. More data will be needed to try to solve this discrepancy.

5. Conclusion

Our study shows a first attempt to monitor the variations of the CO mixing ratio on a given martian location as a function of the solar longitude, using the CO (2−0) band at 2.35 μm. While the band appears to be too weak for a complete mapping of CO, it can be seen that, over Hellas, the CO signature is strong enough for such a study to be performed. Our results indicate a distinct enhancement of the CO mixing ratio over Hellas at the end of southern winter, which seems to confirm the trend indicated by the GCM predictions. It is interesting to note that, in contrast with the case of argon, for which seasonal variations are much stronger than predicted, both the observed and predicted enhancement factors of CO are about a factor 2. One should remember, however, that the argon measurements are performed over the polar cap and not over the Hellas basin, and that enhancement factors may be different over these two locations. In the future, data acquired by OMEGA/MEx during the next martian year will be used to confirm and complement the present study.

Acknowledgements. We wish to thank R. T. Clancy for helpful comments regarding this paper.

References

Billebaud, F., Maillard, J.-P., Lellouch, E., & Encrenaz, T. 1992, A&A, 261, 647
Billebaud, F., Rosenqvist, J., Lellouch, E., et al. 1998, A&A, 333, 1092
Clancy, R. T., Muhleman, D. O., & Berge, G. L. 1990, J. Geophys. Res., 95, 14543
Clancy, R. T., Sandor, B. J., Moriano-Schieven, G. H., & Smith, M. D. 2006, Second International Workshop on Mars Atmospheric Modelling and Observations, Granada, Spain, Feb. 27−March 3, 2006
Encrenaz, T., Melchiorri, R., Fouchet, T., et al. 2005, A&A, 441, L9
Forget, F., Hourdin, F., Fournier, R., et al. 1999, J. Geophys. Res., 104, 24155
Forget, F., Montabone, L., & Lebonnois, S. 2006, Second International Workshop on Mars Atmosphere Modelling and Observations, Feb. 27−Mar. 3, 2006, Abstract 4.2.2
Kakar, R. K., Walters, J. W., & Wilson, W. J. 1977, Science, 196, 1090
Kaplan, L. D., Connes, J., & Connes, P. 1969, ApJ, 157, L187
Krasnopolsky, V. A. 2002, J. Geophys. Res., 108, E2, 4
Lellouch, E., Paubert, G., & Encrenaz, T. 1991, Plan. Space Sci., 39, 219
Melchiorri, R., Encrenaz, T., Fouchet, T., et al. 2006, Plan. Space Sci., in press
Ockert-Bell, M. E., Bell, J. F., Pollack, J. B., et al. 1997, J. Geophys. Res., 102, E4, 9039
Sprague, A. L., Boynton, W. V., Kerry, K. E., et al. 2004, Science, 306, 1364